Nucleation and interface chemistry of ZnO deposited on 6*H*-SiC

A. B. M. A. Ashrafi,[1,*] Y. Segawa, K. Shin,[2] and T. Yao[2]
[1]*RIKEN Photodynamics Research Center, Sendai 980-0845, Japan*
[2]*Interdisciplinary Research Center, Tohoku University, Sendai 980-8578, Japan*
(Received 6 March 2005; revised manuscript received 16 May 2005; published 3 October 2005)

Self-assembled ZnO islands were nucleated on Zn-passivated 6*H*-SiC substrates under the compressive strain. The driving force $\Delta a/a$ and surface energy are the key parameters for the formation of islands and transition to coalescences/grains and a considerable modification of the band structure and structural properties of ZnO epilayers. Transmission electron microscopy (TEM) reflected defects near the ZnO/SiC heterointerfaces that have extended along the ZnO growth direction to be $\leqslant$130 nm, while the high-resolution TEM diffracted the polycrystalline interlayer in the ZnO/SiC heterointerface to be 2–3 nm. Formation of polycrystalline interlayer and columnar growth mode along the [0001] has been attributed to the accumulation of misfit dislocations, dangling atomic bonds, and imbalanced charge distribution in the II-VI/IV materials system, together with complex impurity matrix interdiffused/contributed from the host material, SiC substrate, and metalorganic precursors.

DOI: 10.1103/PhysRevB.72.155302 PACS number(s): 68.55.Ac, 68.55.Ln, 68.37.−d, 81.05.Dz

I. INTRODUCTION

An explosive expansion of research onto ZnO semiconductor material has continued for the fabrication of blue to ultraviolet light emitting diodes (LEDs) and exciton- and polariton-based laser diodes (LDs).[1] Bulk ZnO is a wurtzite wide and direct band-gap material, and the exciton (E_x^b) and biexciton (E_{xx}^b) binding energies are 60 and 15 meV, respectively. Fundamental properties of ZnO, MgO and CdO materials are plotted in Table I. The excitonic properties of ZnO overwhelm GaN by two and a half times since the E_x^b and E_{xx}^b for GaN are 24 and 9 meV, respectively. It has been demonstrated that the E_x^b and E_{xx}^b of bulk ZnO will be enhanced further in the epitaxy to ~120 and ~30 meV, respectively.[2] These promising features of epitaxial ZnO layers will contribute to optoelectronic devices operated at room temperature (RT). It has already been demonstrated the ZnO homoepitaxial LED operated at RT which has ten times longer lifetime than that of the GaN.[3]

Typically, the device quality of epitaxial layers critically depends on its strain, dopants, and nucleation. Nucleation normally reflects the interface geometry due to under layers under the critical thickness and hence, in principle, originates biaxial strain and related defects in heterostructures by the lattice (δ) and thermal (σ) misfits.[4] The strain induces, for example, dark-line defects and piezoelectric devices which tend to shorten the device lifetime by containing a huge density of misfit and threading dislocations including cracking.[4] These defects, in principle, led to the failure of lasers and breakdown of *pn* junctions.[5,6] To overcome those physical and technical limitations in ZnO material for device operation requires a clear understanding on the nucleation and related interface chemistry. Unfortunately, no such systematic studies have yet been demonstrated on the ZnO due to a lack of closely lattice- and thermally matched substrates.

In this paper, nucleation and interface chemistry of ZnO/SiC heterostructures have been addressed. Self-assembled ZnO islands were nucleated and switched to coalescences as well as grains with the increase of deposited layer thicknesses. The growth mode switching critically depends on the accommodated strain relaxation due to the increase of crystallite sizes. Transmission electron microscopy

TABLE I. Most important and fundamental properties of ZnO, MgO, and CdO materials.

	Wurtzite ZnO
Band-gap energy	E_g(RT)=3.37 eV
Exciton binding energy	E_x^b=60 meV
Bohr radius	a_B=18 Å
Lattice constants	c=5.205 Å
	a=3.246 Å
Thermal conductivity	k=40 W/mK
Index of refraction	n=2.0
Stiffness constants	C_{11}=206 GPa
	C_{13}=105 GPa
	C_{33}=211 GPa
	Wurtzite MgO
Band-gap energy	E_g(RT)=5.20 eV
Lattice constants	c=5.086 Å
	a=3.199 Å
Thermal conductivity	k=42 W/mK
Index of refraction	n=1.71
Stiffness constants	C_{11}=297 GPa
	C_{12}=96.5 GPa
	C_{44}=155.7 GPa
	Wurtzite CdO
Band-gap energy	E_g(RT)=2.24 eV
Bohr radius	a_B=12 Å
Lattice constants	c=5.892 Å
	a=3.66 Å
Index of refraction	n=2.49

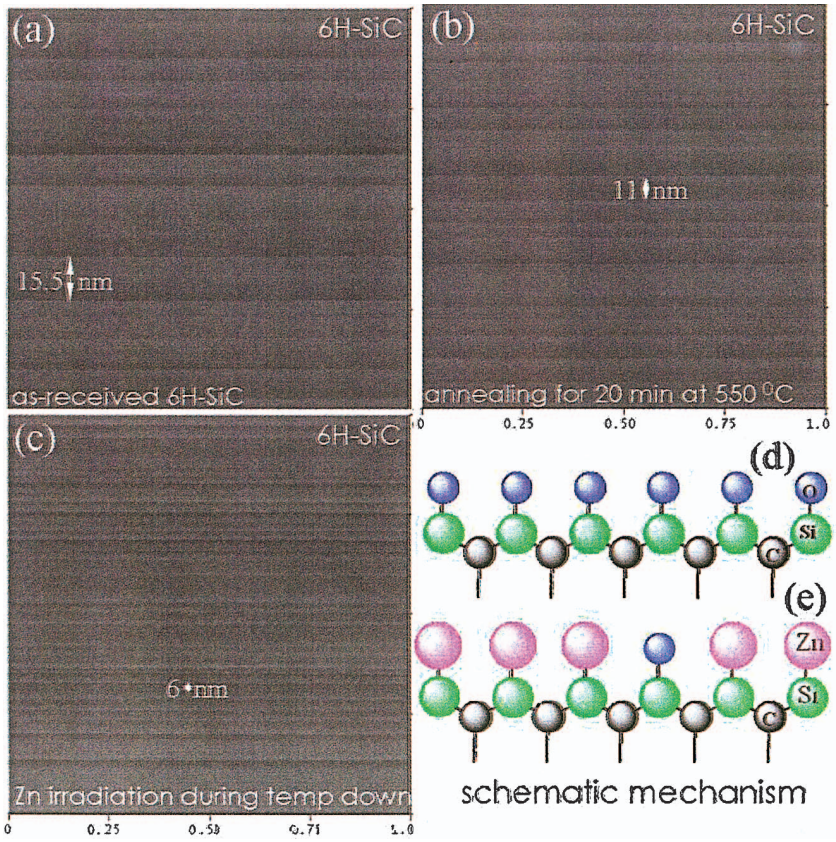

FIG. 1. (Color) 6*H*-SiC substrate cleaning in MOCVD reactor: (a) as-received, (b) post-growth annealed at 550 °C for 20–30 min, (c) irradiation of DEZn during the substrate temperature down from 550 to 475 °C (T_g) and a schematic representation of atomic SiC surfaces with (d) partial oxidation and (e) Zn passivation.

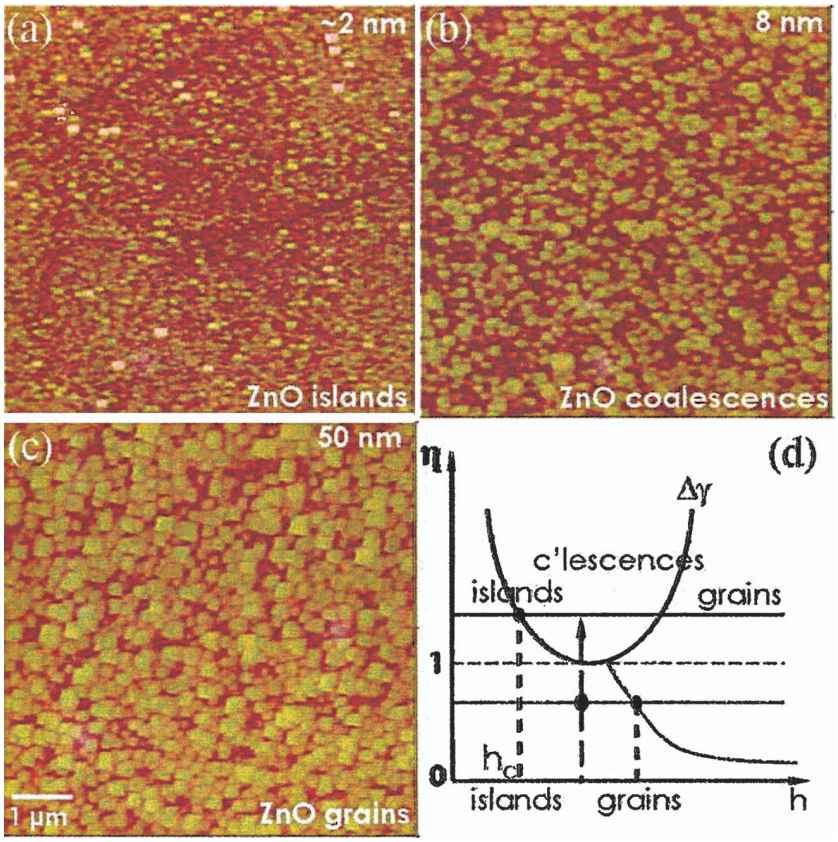

FIG. 2. (Color) Thickness-dependent ZnO layers deposited on the atomically flat terraces of SiC substrates for the layer thickness of (a) ~2 nm, (b) 8 nm, (c) 50 nm, (contact-mode AFM images), and (d) a schematic diagram of the growth mode transition. The η is the ratio in between the two critical thicknesses as $\eta = h_{\text{coalescence}}/h_{\text{island}}$ since the misfit dislocation occurs while the growth mode transforms from islands to coalescences/grains.

(TEM) exhibited a high-density of defects in ZnO/SiC heterointerfaces that decreased rapidly with increasing distance away from the interface, while high-resolution lattice-image diffracted the polycrystalline interlayer due to complex interface chemistry accommodated due to misfit dislocations and dangling atomic bonds, together with complex impurity matrix interdiffused from the host material, SiC, and metalorganic precursors.

II. EXPERIMENTS

ZnO layers were deposited on 6*H*-SiC(0001) substrates by metal-organic chemical-vapor deposition (MOCVD). The details of chemical cleaning and processing have been discussed elsewhere.[7,8] For ZnO deposition, the flow rate of diethyl zinc (DEZn) was controlled by adjusting the flow rate of carrier gas N_2. The substrate temperature was then increased to the selective growth temperature of 475 °C (T_g) for the successive growth of ZnO layers on the 6*H*-SiC substrates. Prior to ZnO deposition, the DEZn was flown first for 40–80 s and then O_2 was flown. The flow rate of DEZn was kept to 6 sccm, while the O_2 flow rate was 10 sccm. The ZnO layer thickness was calibrated using Surface Profiler, Alpha-step 500. To avoid thickness fluctuation error, each sample was carefully calibrated and instrumental error was recorded on an average to be ±1–3 nm.

The *c* axis and *a* axis lengths of ZnO layers were determined by x-ray diffraction (XRD) using the triple-axis $\omega-2\theta$ scans on the (002) and (205) reflections, respectively. The depth profile measurements were performed along the growth direction of ZnO layers by secondary ion-mass spectroscopy (SIMS) using a double-focused ion microanalyzer configured for O^{+2} primary ion bombardment. The quantification of elemental concentration for this instrument was accounted without any relative doses of impurity implants since there are no standard samples yet to compare the ZnO/SiC heterostructure. Two orthogonal $[11\bar{2}0]$ and $[10\bar{1}0]$ cross-section specimens were prepared for TEM examination using the standard procedures and thinned by Ar^+ ion milling. The microscopy was performed using a JEOL 200CX operated at 200 kV and a JEOL 4000EX operated at 300 kV.

III. RESULTS AND DISCUSSIONS

In principle, the atomic configuration of (0001) 6*H*-SiC substrate surface is terminated by Si atoms. As-received Si-faced SiC substrates were dim with multidimensional scratches and nanoscale fluctuations with irregular terrace steps of ~15.5 nm studied by contact-mode atomic force microscopy (AFM), shown in Fig. 1(a). To recover and/or minimize those surface defects and for a well-ordered surface with regular terraces, the SiC substrates were first treated thermally without any reactants at the substrate temperature of 550 °C for 20–30 min. Under these treatments, the surfaces became bright with the visible partial regular terrace heights of ~11 nm. These results suggest that the defects and/or O atoms desorbed partially/completely from the outermost Si atoms from the thermally treated SiC surfaces. Figure 1(b) shows the thermally treated SiC substrate with their minimal terrace heights. In consequences to these procedures, the surface step heights were reduced with the regular terrace steps under the irradiation of DEZn during the substrate temperature down from 550 to 500 °C to be ~6 nm, shown in Fig. 1(c). The surface is seen here almost flat and made up of regular terraces for ~6 nm. It is noted that by oxygen irradiation the thermally treated SiC substrates were backed to the as-received conditions by indicating the presence of oxide layer with irregular scratches and fluctuations.

An observation of regular step heights and terraces in SiC substrate by thermal and the subsequent DEZn irradiation has been summarized by schematic models. The as-received SiC substrates are dominated by oxide layer as shown in Fig. 1(d) that has been confirmed by flowing oxygen on the thermally treated substrates. Under the proper chemical and thermal treatments, the oxide layer desorbs with bare Si atoms. By DEZn irradiation after the thermal treatment, however, on the bare Si atoms, the Si-faced SiC surface is passivated by dangling Zn bonds represented in Fig. 1(e). Therefore, under the thermal treatment as well as the subsequent DEZn irradiation establishes the Zn—Si bonds in the heterointerfaces and hinders the formation of oxidation in nucleation prior to ZnO deposition.

Figures 2(a) and 2(b) show the partial and/or complete coverage of ZnO deposited on the Zn-passivated SiC substrates diffracted in contact-mode AFM observation. For the ZnO layer thickness of $\leqslant 2$ nm, Fig. 1(a) exhibits a partial coverage of ZnO islands with the substrate background. The shape of these islands is polygonlike with flat tops, normally dominated in the cubic semiconductors where the islands are rounded or faceted.[9] This may result from the surface energy anisotropy where the wurtzite ZnO surfaces and the islands prefer a flat-top shape to minimize the total surface energy according to the Wulff construction.[10] With the increase of ZnO layer thickness, however, each island makes contact with its neighbors giving evidence to coalescence and finally to the grains morphology, shown in Figs. 2(b) and 2(c). Presumably, these are the three-dimensional columnar grains typically observed in the various thin films.[11,12]

To explain the experimental growth mode transitions in the ZnO/SiC heterostructures, we have considered a model taking into account the critical thickness and surface energy in Fig. 2(d). In this approach, there are two critical thicknesses dominating as $h_{\text{coalescence}}=E_{\text{coalescence}}/M\delta^2 d$, where $E_{\text{coalescence}}$ is the formation energy per unit length of misfit dislocation during the transition from islands to coalescences/grains, M is the biaxial modulus of the film, and d is the distance between islands-coalescences structures ($d\propto 1/\delta$) and $h_{\text{island}}=\Delta\gamma/M\delta^2\alpha$, where $\Delta\gamma$ is the cost in surface energy associated with creation of island facets ($\Delta\gamma=\gamma_{\text{coalescence}}-\gamma_{\text{island}}$) and α the gain in energy by accommodating the strain of the film through free surfaces. The growth mode transition from islands to coalescences/grains can be described by the ratio η, normally predicts which growth mode favors in epitaxy between the two critical thicknesses as $\eta=h_{\text{coalescence}}/h_{\text{island}}=\alpha E_{\text{coalescence}}/\Delta\gamma d$, which is proportional to $\eta\propto E_{\text{coalescence}}|\delta|/\Delta\gamma$.[13] It is expected that the ZnO/SiC heteroepitaxy establishes equilibrium by the formation of coalescence by minimizing the $\Delta\gamma$

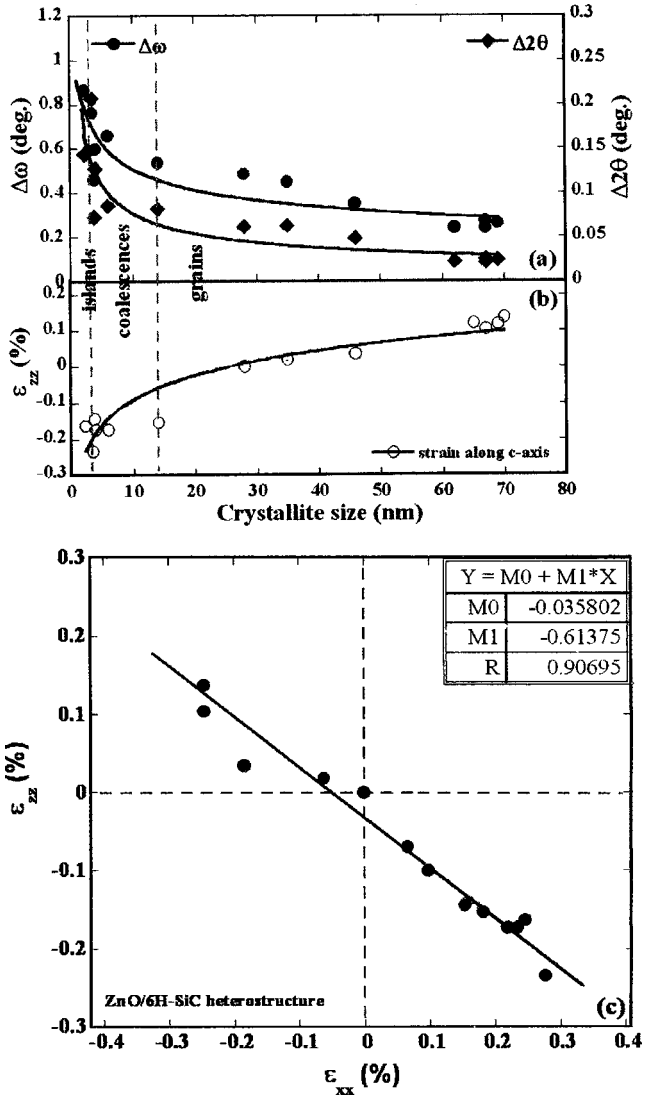

FIG. 3. (a) $\Delta 2\theta$ and $\Delta\omega$ and (b) out-of-plane strain ε_{zz} as a function of crystallite size, and (c) the ε_{zz} versus ε_{xx} deformation of ZnO layers. With the increase of ZnO layer thickness, the strain is significantly relieved. The solid lines are the least-square fits of data taken from XRD and AFM measurements.

as shown in the schematic. With the increase of ZnO layer thickness, however, the coalescence growth mode switched to grains, virtually free from the strain accommodated due to the δ and σ values of $\sim 5\%$ and 1%, respectively. Thus, the $\Delta\gamma$ is low for creating islands/facets, favoring the islands to coalescences/grains transition in ZnO/SiC heteroepitaxy. As the islanding or crystallite size becomes more severe, a larger number of dislocations terminate at island edges by grains. This paradigm is embodied in the nanoheteroepitaxy approach where the strain energy is reduced by leveraging the high, three-dimensional (3D) compliance of nanoscale features.[14]

Figures 3(a) illustrates the variation of x-ray radial axis $(2\theta-\omega)$ and rocking curves $(\Delta\omega)$ and 3(b) out-of-plane strain (ε_{zz}) as a function of crystallite size. The ZnO crystalline sizes were determined from the section analysis of AFM measurements. The $\Delta 2\theta$ reflects broadening due to variations in the Bragg plane spacing and hence, the distribution of strain, while $\Delta\omega$ reflects broadening due to the microscopic tilts of the plane. With the increase of crystallite sizes, the $\Delta 2\theta$ and $\Delta\omega$ decrease suddenly for the average crystalline size of ~ 5 nm and then decrease gradually for the bigger grain sizes diffracted in AFM section analysis. Correlation in between growth modes and strain energies due to crystallite sizes has been marked in Figs. 3(a) and 3(b). These results disclose a clear role of strain relaxation (ε_{zz}) mechanism that is also reflected in Fig. 3(b) as a function of crystallite size. It is noteworthy that the strain energy in the initial growth stage is as large as -2.4%. This indicates that the islands are grown under the high strain energy on the SiC, mostly due to the layer/substrate misfits. The strain, however, decreases drastically with the increase of ZnO layer thickness and gradually relieves afterward. It has been demonstrated that the strain energy also critically depends on the layer thickness, and relieves $\sim 94\%$ at larger grain sizes for the ZnO layer thickness of 1.5 μm.[8]

To understand the state of strain in the ZnO/SiC heteroepitaxy, the in-plane (ε_{xx}) and out-of-plane (ε_{zz}) lattice deformations are plotted in Fig. 3(c). The strain parameters here range from +0.15 to −0.28, and the linear regression of these experimental data leads to a slope of −0.61. This is fairly in agreement with the elastic deformation theory $(-2C_{13}/C_{33})$ using the values of elastic stiffness coefficients plotted in Table I to be −0.99. This elastic deformation constant contrast in between experimental and theoretical values is not clear at this moment. Since the δ and σ in the ZnO/SiC heterostructure are larger, the strain relaxation would imply the elimination of dislocations for a few nanometer-thicknesses and terminated by big crystallite sizes. The stress-strain relations for a hexagonal crystal ($C_{6\nu}$ symmetry) are expressed by a 6×6 matrix. However, if the crystal is strained in the (0001) plane and is free in the [0001], there are only three nonvanishing strain components given by $\boldsymbol{\varepsilon}_{xx}=(a-a_0)/a_0$, $\boldsymbol{\varepsilon}_{yy}=(b-a_0)/a_0$ and $\boldsymbol{\varepsilon}_{zz}=(c-c_0)/c_0=-C_{13}/C_{33}(\boldsymbol{\varepsilon}_{xx}+\boldsymbol{\varepsilon}_{yy})$.[15] Here the subscript "0" indicates the lattice constants of the unstrained crystal and a, b, and c are the lattice constants of the strained crystal and C_{ij} are the elastic constants. In a pseudomorphic epilayer $(a=b)$, the strain can be written as $\boldsymbol{\varepsilon}_{xx}=\boldsymbol{\varepsilon}_{yy}=(a_{\mathrm{sub}}-a_0)/a_0$ and $\boldsymbol{\varepsilon}_{zz}=-2(C_{13}/C_{33})\boldsymbol{\varepsilon}_{xx}$. If the stress is uniaxial $(\sigma_{xx}\neq 0)$ and all the other stress components are zero, the nonzero strain components are given by

$$\begin{pmatrix}\boldsymbol{\varepsilon}_{yy}\\ \boldsymbol{\varepsilon}_{zz}\end{pmatrix}=\frac{1}{C_{13}^2-C_{11}C_{13}}\begin{pmatrix}C_{12}C_{33}-C_{13}^2\\ C_{11}C_{13}-C_{12}C_{13}\end{pmatrix}\boldsymbol{\varepsilon}_{\mathrm{xx}}. \qquad (1)$$

Under the approximation of strain-dependent properties, the isotropic spin-orbit coupling, band structure, and electronic properties of semiconductors are considerably modified. These are in good agreement with our optical measurements where the free, neutral-donor, and acceptor-bound excitons (FX_{A}, D^0X and A^0X) energies of ZnO layers deposited on 6*H*-SiC substrates were blueshifted to 2.5, 4.8, and 5.8 meV, respectively.[16]

TEM cross section of ZnO/SiC heterostructure is represented in Fig. 4(a). The inset shows the transmission electron

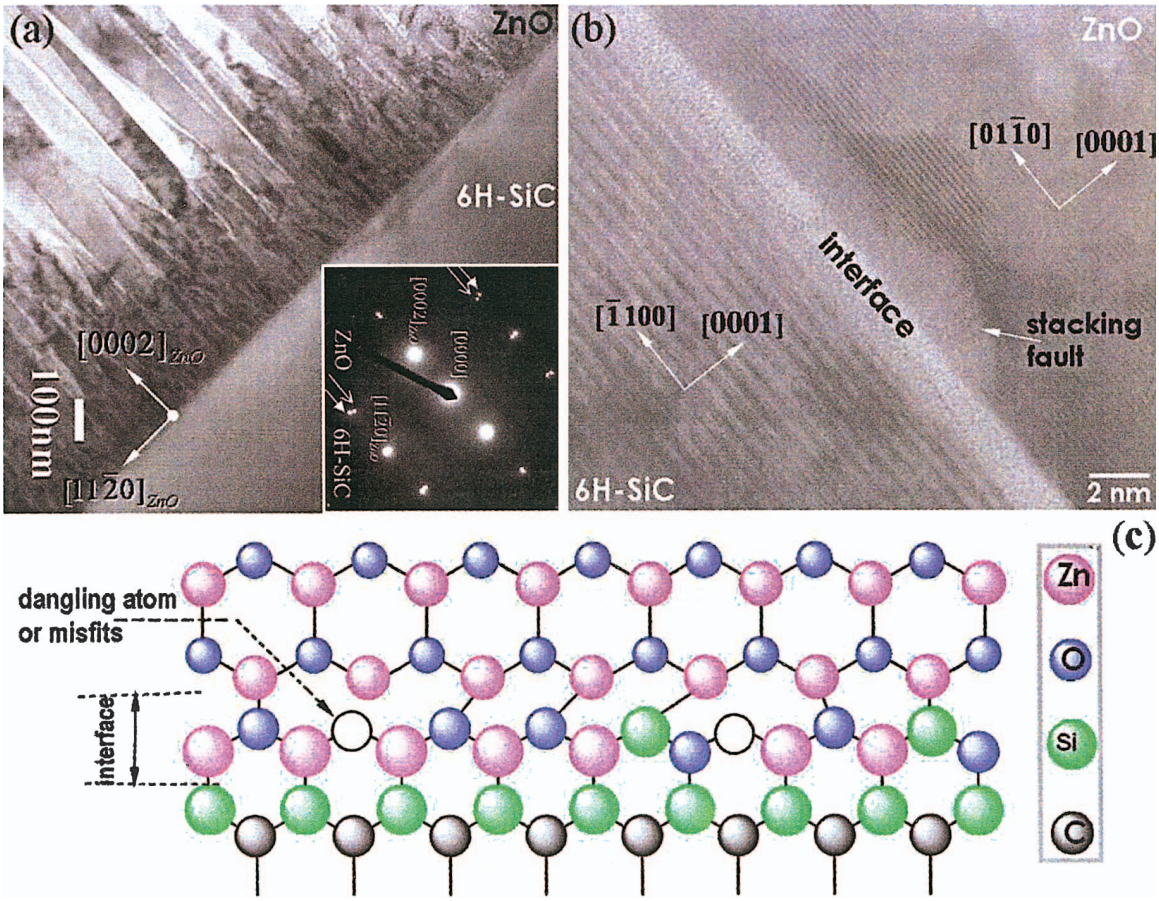

FIG. 4. (Color) (a) TEM cross section of ZnO/SiC heterostructure and TED pattern in the inset and (b) high-resolution TEM lattice image of ZnO/SiC interface. (c) Possible atomic configuration for the ZnO/SiC heterointerface is sketched based on the AFM and TEM evidences.

diffraction (TED) pattern with an epitaxial relationship in the ZnO/SiC heterostructure to be $(0001)_{ZnO}\|(0001)_{SiC}$ and $[11\bar{2}0]_{ZnO}\|[11\bar{2}0]_{SiC}$. The cross section exhibits the columnar growth mode aligned along the [**0001**] and the interface between the epilayer and substrate is rather coherent, although the 6*H*-SiC substrate surface contains nanoscale fluctuations and scratches, which, in principle, play an important role in formation of defects in the ZnO epilayers. A high density of defects was observed near the interface and extended into the ZnO epitaxial layers from the interface to be $\leqslant$130 nm. Since the misfit strain is compressive, misfit dislocations will be created by absent rows of atoms at the heterointerfaces and lead to dips in the surfaces, causing the appearance of dark filamentous features which constitute the subatomic roughness.

Figure 4(b) shows a high-resolution TEM lattice image of ZnO/SiC heterointerface carried out along the $[11\bar{2}0]_{ZnO}$ projection which encloses an angle of 30° with the $[1\bar{1}00]_{ZnO}$ projection. The domain structures near the interface are difficult to detect because a high density of stacking faults parallel and perpendicular to the substrate is accommodated. The density of the stacking faults perpendicular to the substrate is visible clearly in Fig. 4(b). A similar stacking fault formation has been demonstrated in the GaN/SiC heterostructure.[17] The ZnO/SiC heterointerface is perfectly aligned to the $[01\bar{1}0]_{ZnO}\|[\bar{1}100]_{SiC}$ although the interface is irregular with polycrystalline interlayer for the thickness to be 2–3 nm. These focus that the ZnO/SiC interfaces appear structurally semicoherent with the misfit dislocations which could be explained in terms of δ between the interplaner spacing along the $[01\bar{1}0]_{ZnO}$ and $[\bar{1}100]_{SiC}$. The δ is calculated with the ZnO bulk lattice as a reference, $\boldsymbol{\delta}=[(a_{SiC}-a_{ZnO})/a_{SiC}]\times\mathbf{100}\%$, where a_{ZnO} and a_{SiC} are the plane spacings with respect to the bulk ZnO and SiC lattices. Presuming that the bulk lattice constant of ZnO is 0.324 nm, the ZnO lattice spacing in the lattice image has been calculated to be $a_{ZnO}=0.215$ nm. Using the SiC bulk lattice constant of 0.308 nm, the lattice spacing for a_{SiC} is 0.204 nm. The difference in spacing between these planes for ZnO and SiC is only 0.11 Å, so that measurement of individual separations is likely to be inadequate. The estimated experimental δ value for the $[01\bar{1}0]_{ZnO}\|[\bar{1}100]_{SiC}$ is to be 4.87%, almost the same as the bulk ZnO/SiC heterostructure value of ~5%.

To address the atomic configuration at the ZnO/SiC heterostructure, possible interface chemistry and physics have been considered and sketched in Fig. 4(c). The SiC substrate is partially passivated by Zn—Si bonds as represented in Fig. 1(e). After the deposition of ZnO on the Zn-passivated SiC surfaces, the intermixing of Si, Zn, and O atoms and δ in

the ZnO/SiC heterointerface lead to the dangling atomic bonds and misfit dislocations, respectively. It has been demonstrated that the atomic intermixing favors to the island formation in the nucleation.[18] The islands would be strained due to the δ and σ, together with the mixed bonding of Zn, O, and Si atoms, and the strain is relieved by the formation of misfit dislocations and stacking faults diffracted in TEM. Clearly visible stacking faults, in addition, in the ZnO epilayer may be responsible for the imbalanced charge distribution in the II-VI/IV materials system. For the ZnO/SiC system, the imbalanced charge distribution can be understood in terms of ZnO in the following electron counting argument: In the ZnO, each Zn (O) atom contributes $\frac{1}{2}(3/2)$ electron to each of the four bonds surrounding it and in bulk Si, each atom contributes exactly 1 electron per bond. At a (0001) interface between the Si and Zn of ZnO, therefore, the interface bonds with each reach a total of 3/2 electrons instead of the 2 electrons required. This discloses that the II-VI/IV interface does not satisfy the electron distribution conditions. Therefore, the imbalanced electron distribution and dangling atomic bonds are responsible for the columnar growth modes and related defects.

To evaluate the impurity doses in ZnO epitaxy and in the ZnO/SiC heterointerfaces, SIMS was conducted since it detects dopants regardless of their site in the crystal lattice, e.g., in the study of impurity activation and dopant diffusion. The depth profile of ZnO/SiC heterostructure plotted in Fig. 5(a) reveals that the dominant impurities in ZnO and SiC are C, Si, Al, N and N, Al, O, respectively. It is noted that the N in the epitaxial ZnO and SiC has been incorporated due to the carrier gas and *n*-type dopant, respectively. In this experiment, C, Si, N, and Al impurities are dominant in the ZnO epitaxy, while O and Al are incorporated in the SiC substrate. It is evident that the O concentration in the interface is lower than the bulk SiC which is in analogy discussed in substrate surface preparation. The role of these impurities in ZnO is still vague although it has been demonstrated that N works as the acceptor, while Al works as the donor in the ZnO material.[3] While the role of these impurities in ZnO is unclear, the higher C concentration is found than that of the Si and N, although Si is the best partner for oxidation. The depth profile also shows that the ZnO/SiC heterointerface contains a narrow additional interlayer in correlation with the TEM observation. Therefore, it is expected that this interlayer may be accumulated due to the complex impurity matrix contributed/interdiffused from the host ZnO material, SiC substrate, and metal-organic precursors, together with the misfit dislocations and dangling atomic bonds.

Figure 5(b) shows the impurity concentration only in the ZnO epitaxy as a function of DEZn flow rate. This clearly addresses that the N concentration is almost constant in the ZnO epitaxy contributed from the carrier gas N_2 in the MOCVD reactor, while Si concentration gradually decreases with the increase of DEZn flow rate. However, the C and Al concentration is rather high compared to the Si and N impurities in the order of $>10^{15}$–10^{16} cm^3. This discloses that the solubility of C atoms into ZnO material be higher than that of the group-V materials, such as N, and may play a crucial role for conductivity types in ZnO epitaxy. It is noted that these anomalous incorporation of impurities in ZnO layers

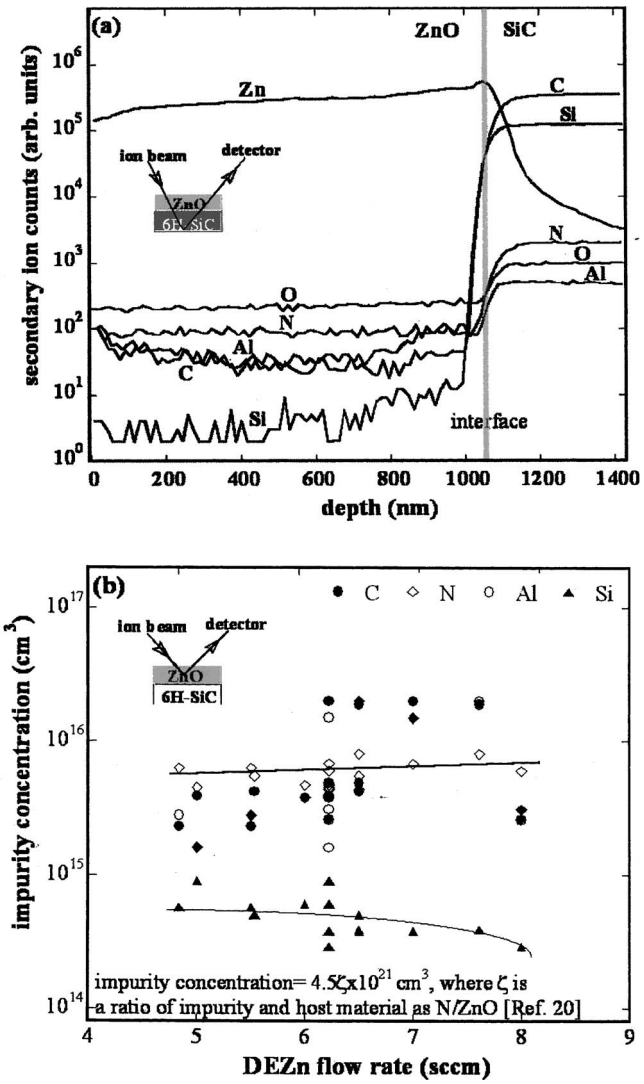

FIG. 5. (a) Depth profile of Zn, O, N, Al, C, and Si in the ZnO/SiC heterostructure. The heterointerface is marked by the shaded line and the respective impurities are represented in Table I and (b) the impurity concentration in ZnO epilayers has been plotted as a function of DEZn flow rate. The solid lines are the least-squares fits of experimental data in (b). The impurity concentration has been calculated from secondary ion counts by using the equation $4.5\zeta\times10^{21}$ cm^3, where ζ is a ratio of impurity and host material as N/ZnO.

are not yet clear since the SiC surface contains nanoscale fluctuations and SIMS were conducted without any relative doses of impurity implants.

An anomalous distribution of impurities in ZnO epitaxy remarks that the solubility of metallic C atoms in ZnO is relatively higher than that of the N and Si. This complex lattice manipulation, together with misfit dislocations and dangling atomic bonds in the ZnO/SiC heterointerfaces lead to the polycrystalline interlayer. This is consistent both in SIMS and TEM analysis as the initial growth of ZnO would not wet the SiC surface due to irradiation of DEZn reactant in the heterointerfaces. This complex interface chemistry can be interpreted in terms of the interface energy by $\gamma_{\mathrm{epi}}=[\delta/(\delta+1)]\gamma_{\mathrm{sub}}$, where γ_{sub} is the surface energy per unit

area of the substrate.[19] The number of atoms per unit area is $N=\mathbf{4}/\sqrt{3}a^2$, where a is the lattice constant of the epilayer and/or the cluster a ($a \geqslant a_{\mathrm{sub}}$) as $a=ka_{\mathrm{sub}}$, where $k=\boldsymbol{\delta}+\mathbf{1}(k \geqslant 1)$. Therefore, the total interfacial energy E can be written as

$$\mathrm{E}=\mathrm{A}\boldsymbol{\gamma}_{\mathrm{epi}}=\mathrm{A}\frac{\boldsymbol{\delta}}{\boldsymbol{\delta}+\mathbf{1}}\frac{\boldsymbol{\Delta}H_{\mathrm{sub}}}{\mathbf{4}\sqrt{\mathbf{3}}a_{\mathrm{sub}}^2 N_A}, \tag{2}$$

where A is the interfacial area of each structure, N_A is the Avogadro's number ($N_A=6.023\times10^{23}$), and ΔH_{sub} is the enthalpy of evaporation per mole of the substrate. This equation clearly indicates the dominant two parameters as δ and γ_{sub}, where γ_{sub} depends on the ΔH_{sub} and a_{sub}. Therefore, these parameters clearly address that the interfacial energy depends on δ as responsible for introducing misfit dislocations and the γ_{sub} responsible for creation of islands, together with the dangling atomic bonds in the ZnO/SiC materials system, represented with the schematic model in Fig. 4(c). It has been assigned that the dangling atomic bonds in the ZnO/SiC heterointerfaces dominate due to misinterplacement of cation-anion lattices. The Zn—Si bonds favor growing islands in nucleation that has preserved due to the DEZn irradiation on the thermally treated SiC surfaces. In addition, Zn—Zn bonds such as a tiny droplet may be formed during the deposition with low O flow rate on ZnO on SiC although the dependence of the interface treatment suggests the polarity of ZnO on Zn/SiC(0001) be ZnO(0001), the confirmation of the surface polarity is required to settle down this issue.

IV. CONCLUSION

In summary, nucleation and interface chemistry of ZnO/SiC heterostructure have been demonstrated. Associated ZnO growth modes depend on the strain energy and surface energy that favor growing islands in nucleation. Complex interface chemistry accommodated in the ZnO/SiC heterointerface is responsible for the formation of misfit dislocations and dangling atomic bonds, together with impurity complex contributed from the host material, SiC substrate, and metal-organic precursors. Higher solubility of C atoms than N may play an informative role in ZnO epitaxy for conductivity type's conversion.

ACKNOWLEDGMENTS

This work was supported in part by the Photodynamics Research Center, and The Institute of Physical and Chemical Research, Japan.

*Corresponding author. Electronic mail: ashrafi@riken.jp

[1] M. Zamfirescu, A. Kavokin, B. Gil, G. Malpuech, and M. Kaliteevski, Phys. Rev. B **65**, 161205(R) (2002).
[2] H. D. Shun, T. Makino, Y. Segawa, M. Kawasaki, A. Ohtomo, K. Tamura, and H. Koinuma, J. Appl. Phys. **91**, 1993 (2002).
[3] A. Tsukazaki, A. Ohtomo, T. Onuma, M. Ohtani, T. Makino, M. Sumiya, K. Ohtani, S. F. Chichibu, S. Fuke, Y. Segawa, H. Ohno, H. Koinuma, and M. Kawasaki, Nat. Mater. **4**, 42 (2005).
[4] S.-H. Lin, D. Shindo, H.-B. Kang, and K. Nakamura, J. Vac. Sci. Technol. B **19**, 506 (2001).
[5] R. F. Service, Science **276**, 895 (1997); B. Gil, O. Briot, and R. L. Aulombard, Phys. Rev. B **52**, R17028 (1995).
[6] T. Nishida and N. Kobayashi, J. Cryst. Growth **221**, 297 (2000).
[7] A. B. M. A. Ashrafi, B. P. Zhang, N. T. Binh, and Y. Segawa, Jpn. J. Appl. Phys., Part 1 **43**, 1114 (2004).
[8] A. B. M. A. Ashrafi, B. P. Zhang, N. T. Binh, and Y. Segawa, Appl. Phys. Lett. **84**, 2851 (2004).
[9] F. Midmann, B. Daudin, G. Feuillet, Y. Samson, J. L. Rouviere, and N. Pelekanos, J. Appl. Phys. **83**, 7618 (1998).
[10] S. H. Jones, L. K. Seidel, K. M. Lau, and M. Harold, J. Cryst. Growth **108**, 73 (1991).
[11] D. J. Eaglesham, J. E. Bower, M. A. Gross, and S. Merchant, Appl. Phys. Lett. **71**, 219 (1997).
[12] J. Lu, L. Haworth, D. I. Westwood, and J. E. Macdonald, Appl. Phys. Lett. **78**, 1080 (2001).
[13] J. M. Gerard, J. B. Jenin, J. Lefebure, J. M. Moisson, and F. Barthe, J. Cryst. Growth **150**, 351 (1995); C. G. van de Walle and J. Neugebauer, Phys. Rev. Lett. **88**, 066103 (2002).
[14] S. Il Park, T. S. Cho, S. J. Doh, J. L. Lee, and J. H. Je, Appl. Phys. Lett. **77**, 349 (2000).
[15] *Group III-Nitride Semiconductor Compounds*, edited by B. Gil (Clarendon, Oxford, 1998).
[16] A. B. M. A. Ashrafi, B. P. Zhang, N. T. Binh, and Y. Segawa, J. Cryst. Growth, **275**, e2439 (2005).
[17] D. Freundt, D. Holz, H. Luth, M. Romani, A. Rizzi, and D. Gerthse, J. Vac. Sci. Technol. B **15**, 1121 (1997).
[18] Li Tie, Li Yu-zhi, Zhang Yu-heng, Gao Chen, Wei Shi-qiang, and Liu Wen-han, Phys. Rev. B **52**, 1120 (1995).
[19] K. Nakajima, Jpn. J. Appl. Phys., Part 1 **38**, 1875 (1999).